DESIGN OF MASS SAVING CONFIGURATIONS FOR WINGED REENTRY VEHICLES

Antonio Viviani, Giovanni Lanzillo, Luigi Iuspa
Seconda Università di Napoli (SUN), via Roma 29, 81031 Aversa, Italy.
antonio.viviani@unina2.it; giovanni.lanzillo@unina2.it; luigi.iuspa@unina2.it

Keywords: *Reentry Vehicle, Aerothermodynamics, Shape Optimization, Genetic Algorithm.*

Abstract

This paper reports the strategy adopted and the methodologies implemented to investigate the problem of the most performing shape for a Winged Re-entry Vehicle (RV-W). The RV-W mission considered is a gliding flight into the descent plane starting from an altitude of 120 km. During the descent both thermal and dynamic quantities are accounted for crew livability and structural integrity. The touchdown velocity, the TPS temperature at wall and the normal load factor and asymptotic dynamic pressure peaks are taken into account as parameters for structural integrity while the TPS inner surface temperature is considered for crew livability. The shape is modeled by a parametric model based on Coons surfaces and a five-parameters law rules the insulating material thickness distribution. The Thermal Protection System (TPS) material considered is Li-900. The three-degree of freedom model for the re-entry trajectory is integrated until the touchdown occurs and a subsonic drag parachute system is foreseen. The thermal state of the surface is calculated under the radiative equilibrium hypothesis and the heat flux at the surface is determined via hypersonic boundary layer relations. The temperature through the TPS thickness is integrated locally with the non-stationary one-dimensional model. Results for a minimum weight configuration optimization performed by a Genetic Algorithm (GA) method are presented.

Nomenclature

C_{he}	Stanton number
c_p	specific heat at constant pressure
D	drag
g	gravity acceleration
L	lift
h	altitude
k	thermal conductivity
m	RV-W mass
q_{gw}	heat flux from gas to wall
$q_{rad,w}$	radiative heat flux at wall
r_n	nose radius
R_Q	Earth radius
t	time
$th_{elem,i}$	TPS thickness of the i-th shape element
T	temperature
T_{lim}	TPS material temperature limit
T_{re}	radiative equilibrium temperature
V	velocity
x	length coordinate
γ	flight-path angle
ε	emissivity coefficient
ρ	density
ϕ	body local angle

1 Introduction

The re-entry vehicle's mission is to transfer the crew from a Low Earth Orbit (LEO) to the Earth's surface safely. The RV-W's potential and kinetic energy has to be dissipated during the re-entry gliding flight. Therefore, the RV-W performs a braking mission intended to reduce its velocity. The RV-W shape and the re-entry trajectory parameters are designed to increase the deceleration at hypersonic/supersonic speed while a system of two subsonic parachutes are considered for the subsonic flight. During the descent, the RV-W has to withstand both thermal and mechanical loads and also in a preliminary design stage a crude esteem of the solicitations is needed. Some papers suggest to evaluate the vehicle dynamic performances by the mean of the aerodynamic efficiency and the ballistic coefficient and to esteem the thermal loads by the integrated heat flux acting on the re-entry vehicle [1][2]. In this work a more detailed esteem of the mechanical and thermal loads acting on the RV-W during the re-entry is proposed: the highest normal load factor, the asymptotic dynamic pressure peak and the touchdown velocity are considered as a measure of the structural solicitations and the thermal load is calculated by a rough but local calculation of the TPS thermal state during the descent.

2 Shape Parametric Model

The shape parametric model is made of *Coons*-surface patches which enclose a non-deformable volume accommodating a four-people crew. A set of 20 topological, dimensional and non-dimensional variables control the cabin layout, the symmetry plane outline, the wing planform and three cross-sections. Some possible shapes are shown in Fig. 1.

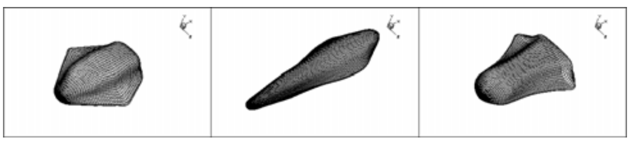

Fig. 1 Examples of Parametric Shapes

For each crew member a 1500x800x1500mm accommodating volume, 20% increased, is foreseen. The crew accommodation is not *a priori* assigned but four potential layouts are considered, as shown in Fig. 2.

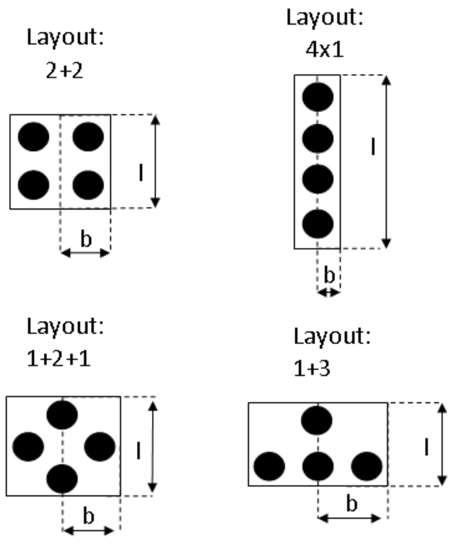

Fig. 2 Crew Potential Layouts

The RV-W wireframe is modeled by a set of parametric B-splines. The forward outline of the symmetry plane is ruled by the control points F_1 and F_2. They are connected to the cabin corners by the upper and the lower line respectively, as shown in Fig. 3.

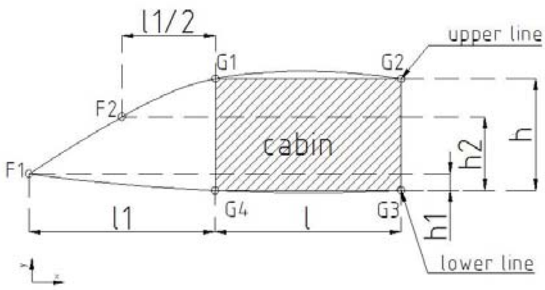

Fig. 3 RV-W Forward Outline of the Simmetry Plane

The F_1 coordinates are controlled by the l_1 and h_1 design variable while F_2 depends on l_1 and h_2. The nose radius in the symmetry plane is defined by a dimensional variable *rnose* controlling the fillet between the upper line and the lower line. The aft symmetry plane outline, shown in Fig. 4, is modeled by two B-splines connecting in the control point F_3.

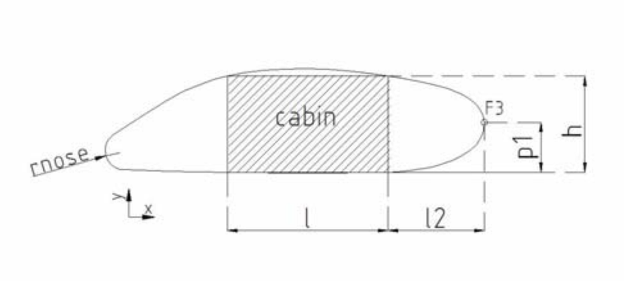

Fig. 4 RV-W Simmetry Plane Outline

As shown in Fig. 5, the wing planform is preliminary designed by a segmented line passing through five control points E_0, E_1, E_2, E_3, E_4 and then smoothed controlling the fillet between the pairs of connected segments. In order to not introduce slightly sensitive variables the wing fillets are realized by a single-parameter routine. The E_i $(i=1,2,3,4)$ ordinates are controlled by a set of non-dimensional parameters, c_i $(i=1,2,3,4)$, while the E_1 abscissa is equal to the semi-wingspan and the E_i $(i=0,2,3,4)$ abscissas are expressed as a duly fraction of k_1. The smoothed wing planform is linked to the RV-W fore and aft by two B-splines.

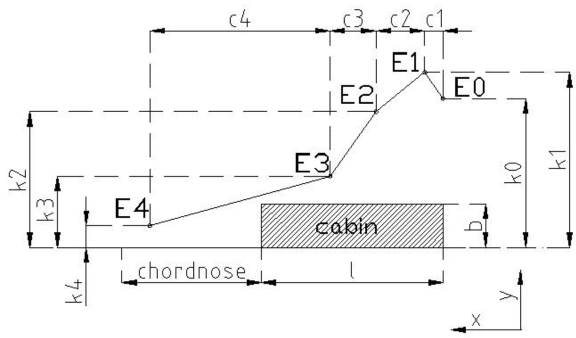

Fig. 5 Wing Planform Segmented Outline

Five parametric cross-sections, statically collocated along the length, complete the RV-W wireframe, as shown in Fig. 6. The most forward and the backward cross-sections are made of a pairs of B-splines connecting the upper line and the bottom line with the wing planform outline while each central cross-section is controlled by a set of non-dimensional parameters which are function of the cabin height and the local wingspan. The cross-section smoothness is regulated by a single parameter acting on all the section fillets.

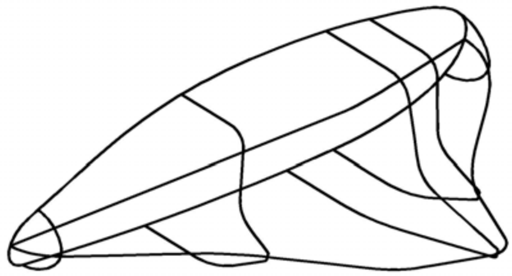

Fig. 6 Half-Model Wireframe

The five cross-sections are sampled and then non-linearly stretched along the windward line, the wing planform outline and the leeward line. As shown in Fig. 7, the shape is discretized by four-vertex panel exploited as both aerodynamic and thermal computational elements.

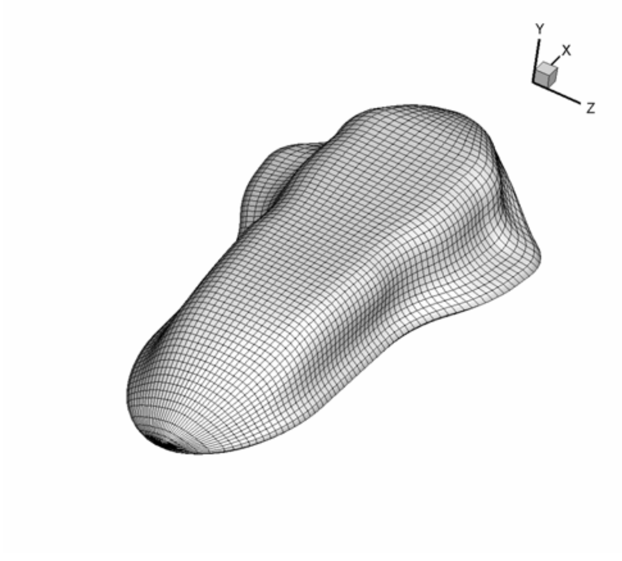

Fig. 7 RV-W Discretized Shape

3 Re-entry Trajectory

The RV-W mission profile considered is a gliding flight in the descent plane as no bank angle is considered, as shown in Fig. 8. The motion is described by the three-degree of freedom model for the re-entry dynamic of a mass point in a planetocentric, considered as inertial, frame:

$$\frac{dV}{dt} = -\frac{D}{m} - g \sin\gamma$$
$$V\frac{d\gamma}{dt} = \frac{L}{m} - g\cos\gamma + \frac{V^2}{R_{\Theta} + h}\cos\gamma \qquad (1)$$
$$\frac{dh}{dt} = V\sin\gamma$$

The RV-W mass is valued via statistical formulas, considering each sub-system separately [11]. The TPS mass is known from its distribution. The aerodynamic coefficients, C_L and C_D, are calculated by the mean of panel method. Furthermore, in order to reduce the touchdown velocity a system of two subsonic parachutes is foreseen and its effect is accounted for a drag increase. The drag parachutes mission profile is the same than Soyuz, the first parachute deploys at 0.8Mach and the second one at 0.25Mach. The RV-W parachute area is linearly mass scaled with Soyuz data. The $C_{D,parachute}$ value assumed is 0.8 [4].

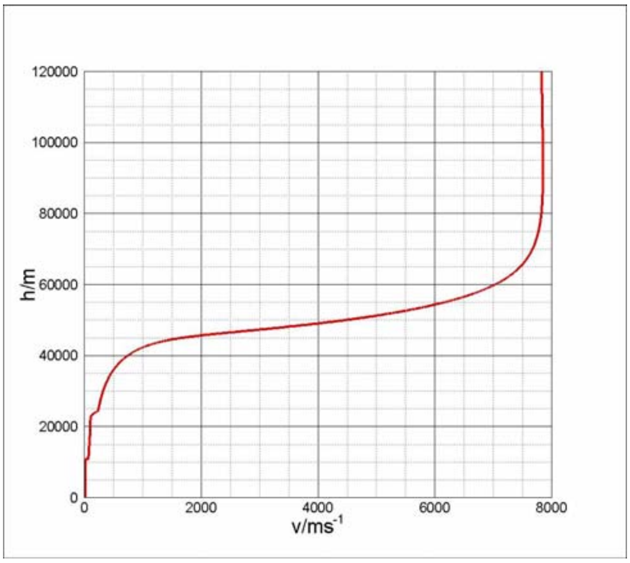

Fig. 8 Re-entry Trajectory Profile

The velocity and altitude initial condition are set considering an atmosphere entry from a de-orbit maneuver at 120km, so they read:

$$h_{t=0} = 120km$$
$$V_{t=0} = 7830ms^{-1} \qquad (2).$$

The initial flight path-angle value, $\gamma(t_0)$, has to be negative to perform a descent flight and it is assumed as a parameter.

4 Thermal Protection System

The Thermal Protection System is modeled with an insulating coating made of LI-900 material whose thermal properties of interest are reported in Table 1, from ref. [5].

Table 1. LI-900 Thermal Properties

ρ	1.44e2kg/m^3
c_p	6.28e2J/kgK
k	4.76e2W/mk
ε	0.88
T_{lim}	1760K

Each four vertex element of the RV-W is considered as a thermal computational element. The insulating material thickness distribution is controlled by a five-parameters law and it naturally assigns a major amount of material to the most thermal stressed areas, *i.e.* nearby the stagnation point and the RV-W windward side. As shown in Fig. 9, the LI-900 coating is ruled by a bi-linear law in the symmetry plane starting from the nose and a linear decreasing law starting from the windward to the leeward side at each RV-W wireframe rib.

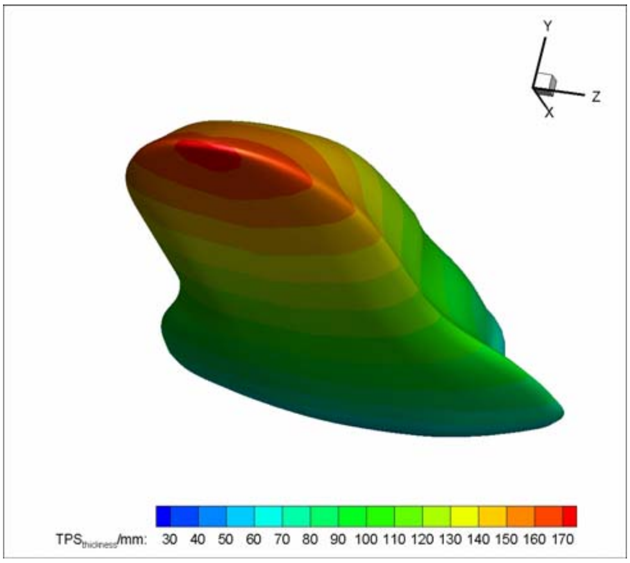

Fig. 9 TPS Thickness Distribution

Each computational element is considered as independent from the surrounding ones, *i.e.* adiabatic side-walls are assumed, and a transient, one-dimensional analysis is performed through the TPS thickness. Furthermore, the whole TPS is considered in thermal equilibrium with the atmosphere at the entry. The wall temperature is calculated according to the radiative equilibrium hypothesis and the TPS inner surface is considered as adiabatic: it is a conservative hypothesis because of the TPS inner surface temperature is an optimization constraint [6]. Therefore, the TPS thermal problem formulates:

$$\begin{aligned} &\rho \cdot c_P \frac{\partial T}{\partial t} th_{ele,i} = k \frac{\partial^2 T}{\partial x^2} \\ &T_{|t=0} = T_{atm|h=120km} = 285K \\ &T(t)_{wall} = T_{re}(t) \\ &\frac{\partial T}{\partial x}(t)_{x=th_{ele,i}} = 0 \end{aligned} \qquad (3).$$

The radiative equilibrium hypothesis takes into account only the heat flux from the gas to the wall, q_{gw}, and the cooling radiative heat flux from the wall to the gas, $q_{rad,w}$, so the heat flux balance at the TPS wall is solved for T_{wall}, as shown in Fig. 10, and it reads:

$$\begin{aligned} &q_{gw} - q_{rad,w} = 0 \\ &q_{gw} = \varepsilon \sigma T_{wall}^4 \end{aligned} \qquad (4).$$

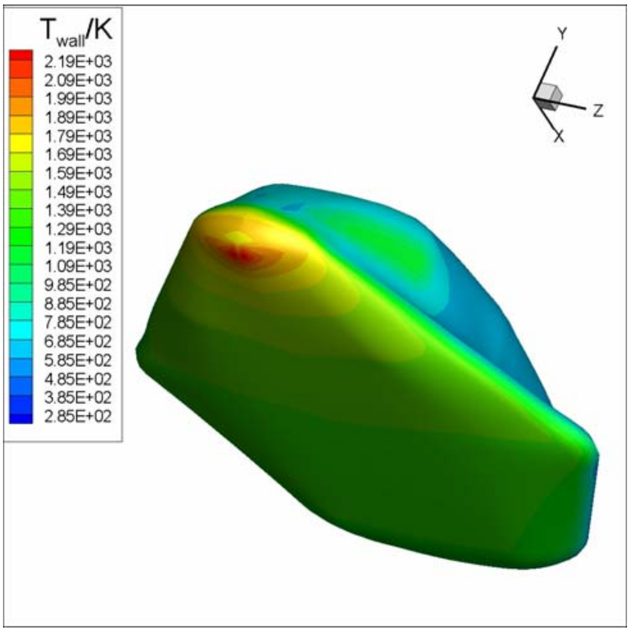

Fig. 10 Wall Temperature Contour

The q_{gw} is evaluated according to the laminar high speed flight formulation proposed in [7]:

$$q_{gw} = C \rho_\infty^N V_\infty^M \qquad (5).$$

The C,N and M quantities read for the stagnation point:

$$\begin{aligned} &M = 3 \quad N = 0.5 \\ &C = (1.83e-4)\, r_n^{-1/2} \left(1 - \frac{c_p T_w}{0.5V^2}\right) \end{aligned} \qquad (6),$$

and for the windward side, locally modeled as a large Angle of Attack (AoA) flat plate:

$$\begin{aligned} &M = 3.2 \quad N = 0.5 \\ &C = k_C(\phi)\left(x^{-1/2}\right)(1 - g_w) \\ &k_C = (2.42e-5)\cos^{\frac{1}{2}}\phi \sin\phi \\ &g_w = \frac{c_p T_w}{0.5V^2} \end{aligned} \qquad (7).$$

The q_{gw} for the leeward surface is modeled via the laminar compressible boundary layer model:

$$q_{gw} = C_{he} \rho_e V_e (T_{aw} - T_w) \qquad (8).$$

The thermal problem time integration is extended until Mach ≤ 2.

5 Constraints Description

The analysis performed takes into account a set of mechanical and thermal quantities evaluated during the descent flight and considered as constraints. The free-flow dynamic pressure, q_∞, is considered a measure of the RV-W structure solicitations as being proportional to aerodynamic forces. Its admissible peak value is 14kPa. The normal load factor is an indicator both of the g-loads acting on the crew and the structural stresses. Its admissible peak value is set to 2.5 [9]. The touchdown velocity is considered and its limit is set to $10 ms^{-1}$. Furthermore, two thermal constraints are taken into account. Considering the Li-900 as insulating material, a maximum allowable TPS temperature is set to 1760K and a maximum TPS interior temperature of 422K has to be fulfilled in order to preserve crew livability condition and the structural integrity.

6 Optimization Procedure for Mass Saving

The aim of the optimization procedure presented is the RV-W mass minimization considering as constraints the free-flow dynamic pressure, the normal load factor, the touchdown velocity and the TPS inner and outer temperature. Both the outer and the interior thermal constraint is naturally vectorial so a proper manipulation is necessary in order to summarize it in a scalar function. The optimization problem formulates as single-objective and constrained and it reads:

$$\begin{gathered} \min!\ m\left(\underline{x}\right) \\ \underline{x_i} \le x_i \le \overline{x_i} \qquad i = 1,\ 2,\ \ldots,\ I \\ g_j^{MIN} \le g_j\left(\underline{x}\right) \le g_j^{MAX} \qquad j = 1,\ 2,\ \ldots,\ J \end{gathered} \tag{9}$$

The parameters array $\underline{x_i}$ controls the RV-W shape, the TPS distribution, the AoA and the initial flight-path-angle. The RV-W mass, $m(\underline{x})$, is the optimization objective function and the constraint functions specify as follows:

$$\begin{gathered} \frac{\max!\ q_\infty}{q_{\infty,\,ADM}} \le 1 \\ \frac{\max!\ n_Z}{n_{Z,\,ADM}} \le 1 \\ \frac{V_{TD}}{V_{TD,\,ADM}} \le 1 \\ T_{P,\,INT} = \sum_{i=1}^{NUMELEM} \left(\max\ T_{i,\,INT} - T_{ADM,\,INT}\right)\delta_i \le 0 \\ T_{P,\,OUT} = \sum_{i=1}^{NUMELEM} \left(\max\ T_{i,\,OUT} - T_{ADM,\,OUT}\right)\delta_i \le 0 \\ \delta_i = \begin{cases} 1 & \max\ T_{i,\,INT(OUT)} > T_{ADM,\,INT(OUT)} \\ 0 & otherwise \end{cases} \end{gathered} \tag{10}$$

The execution flow, represented in Fig. 11, shows that at first the geometrical model is calculated, then the TPS and the RV-W mass is esteemed. Once the shape is defined, its aerodynamic characteristics are computed and then the re-entry trajectory is integrated. Finally, the wall temperature is evaluated, the TPS thermal state solved and the constraint functions calculated.

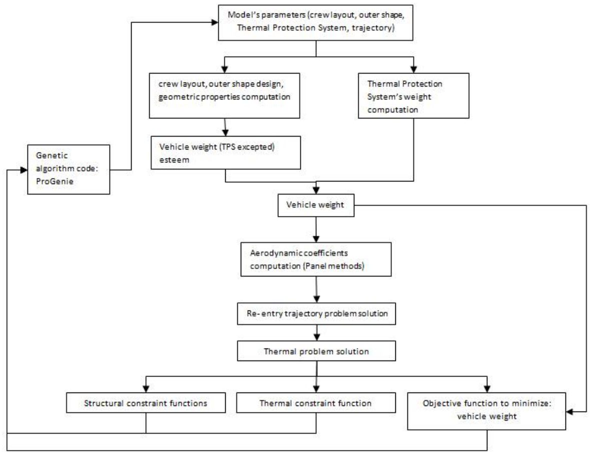

Fig. 11 Optimization Procedure Execution Flow

A GA method implemented in *ProGenie* is exploited as optimizer [10]. The GA fitness function specify as follows:

$$\begin{gathered} fitness\left(\underline{x}\right) = \frac{m_{TEO} - m\left(\underline{x}\right)}{\prod_{j=1}^{J} k_j\left(\underline{x}\right)} \\ g_1\left(\underline{x}\right) = \left(\frac{g_j^{\max} - g_j\left(\underline{x}\right)}{g_j^{\max} - g_j^{\min}}\right)^{H_j} \\ g_2\left(\underline{x}\right) = \left(\frac{g_j\left(\underline{x}\right) - g_j^{\min}}{g_j^{\max} - g_j^{\min}}\right)^{H_j} \\ k_j\left(\underline{x}\right) = \begin{cases} g_1\left(\underline{x}\right) & g_j\left(\underline{x}\right) < g_j^{\min} \\ 1 & g_j^{\min} \le g_j\left(\underline{x}\right) \le g_j^{\max} \\ g_2\left(\underline{x}\right) & g_j\left(\underline{x}\right) > g_j^{\max} \end{cases} \end{gathered} \tag{11}$$

Since *ProGenie* searches for the maximum of the objective function a theoretical mass value, m_{TEO}, high enough to make the difference $m_{TEO}-m(\underline{x})$ always positive is necessary. Finally, the computational cost of a single configuration is reduced as much as possible in order to make the optimization procedure affordable. Therefore, a massive use both of array programming for the simultaneously analysis of the TPS elements thermal state and for the geometry properties calculation in *Ansys Design Parametric Language (APDL)* and of compiled language, *C Language*, for the sequential routines is made. As result, a single configuration analysis time lasts less than fifteen seconds on an entry-level WorkStation equipped with two Xeon 6-core.

Results

The results presented are obtained from an optimization run whose GA general settings are reported in Table 2.

Table 2. GA general settings

Number of generations	80
Individuals per standard population	50
New individuals at each generation	50
Selection Operator	Roulette Wheel
Crossover Operator	Crossover Single Cut
Mutation Operator	Yes, dynamic
Starting Population	Extended
Fitness Scaling	Cosine Law

The time histories are about the most performing individual at each generation. For the sake of brevity, only the most meaningful design variables are shown and their range are reported in Table 3.

Table 3. Range of Design Variables

l_1	2500mm	5000mm
l_2	600mm	1600mm
k_o	0.5	0.8
$k_{\backslash}$	1200mm	2000mm
k_2	0.5	1
k_3	0.2	0.4
k_4	0.6	0.9
c_1	0.05	0.35
c_2	0.2	0.6
c_3	0.4	0.85
c_4	0.3	0.7
H_1	0.05	0.3
P_1	0.2	0.7
r_n	10mm	300mm
α	35deg	42deg

The crew layout is the 2+2 type, for the most. The time histories of the variables l_1, l_2 and r_n are reported in Fig. 12, Fig. 13, Fig. 14.

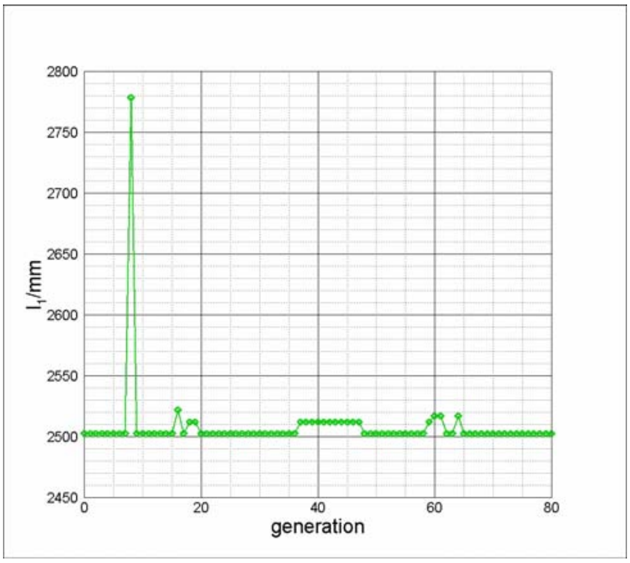

Fig. 12 l_1 time history

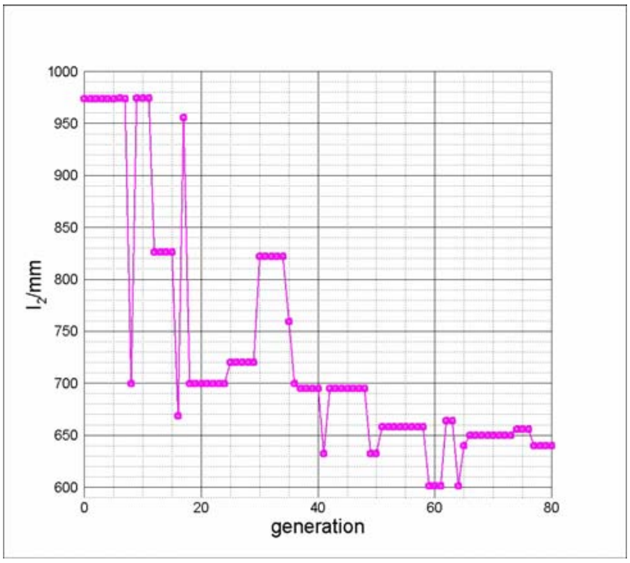

Fig. 13 l_2 time history

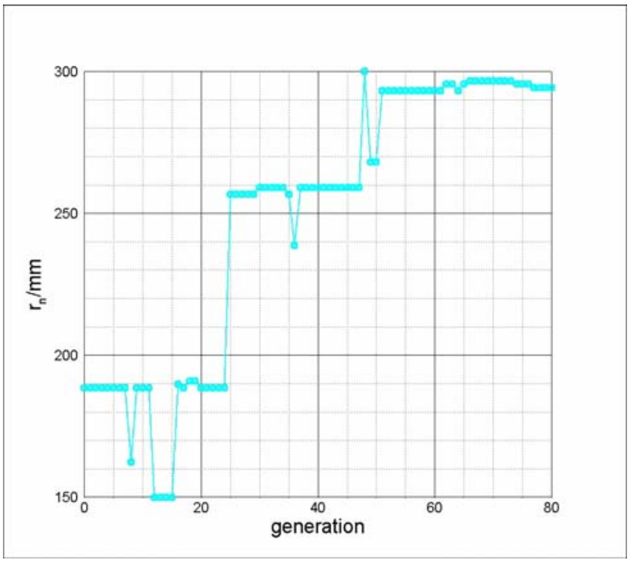

Fig. 14 r_n time history

The variables H_1 and P_1, represented in Fig. 15, are expressed as fraction of the cabin height h_0.

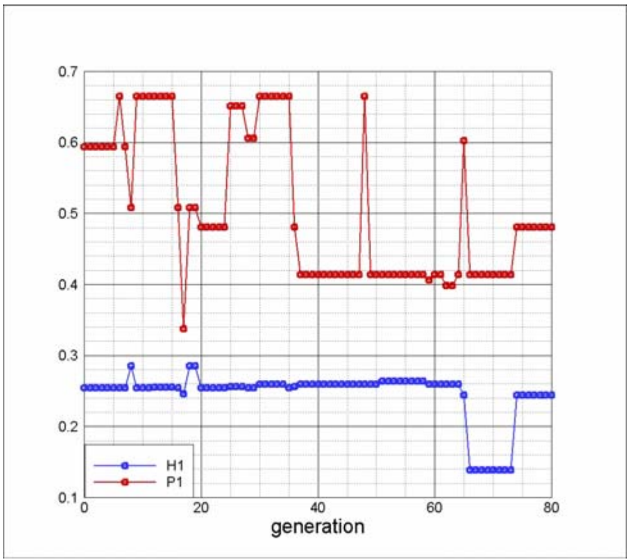

Fig. 15 H_1 and P_1 time histories

The main design variables for the wing planform are shown in Fig. 16, Fig. 17, Fig. 18.

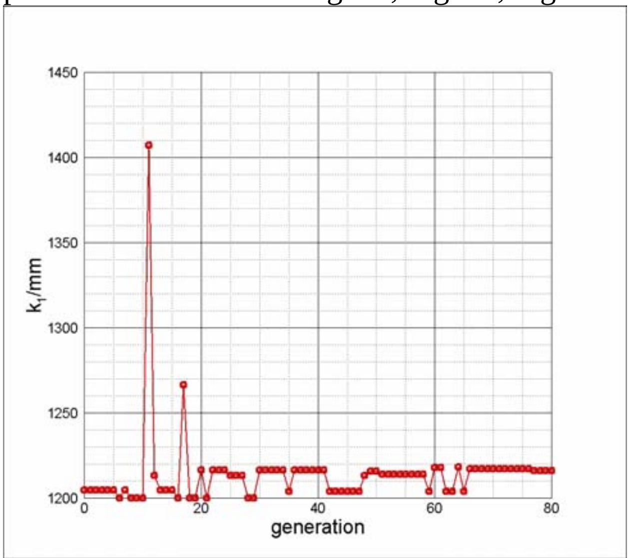

Fig. 16 k_1 time history

The time history of the RV-W mass is reported in Fig. 19. As expected, the main changes in configuration are made in the first tenths of generations with an higher rate of decrease of the RV-W mass while in the lasts only little improvements happen. In Fig. 20, Fig. 21, Fig. 22 and Fig. 23 are shown the shape for the best individuals at the 0^{th}, 20^{th}, 40^{th} and 60^{th} generation.

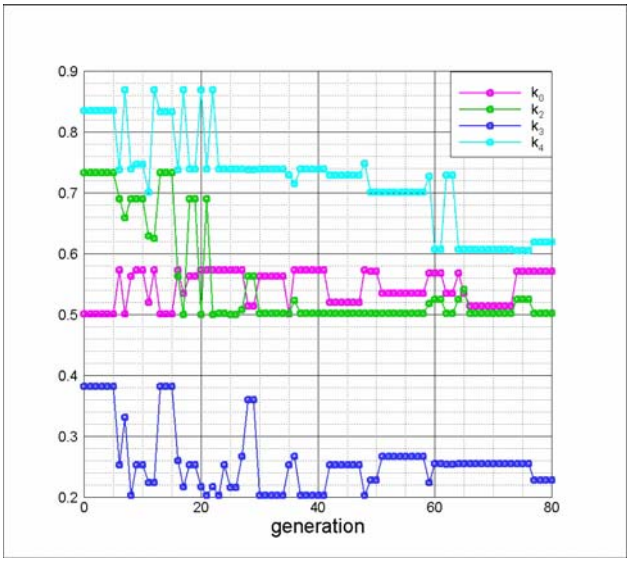

Fig. 17 k_0, k_2, k_3 and k_4 time histories

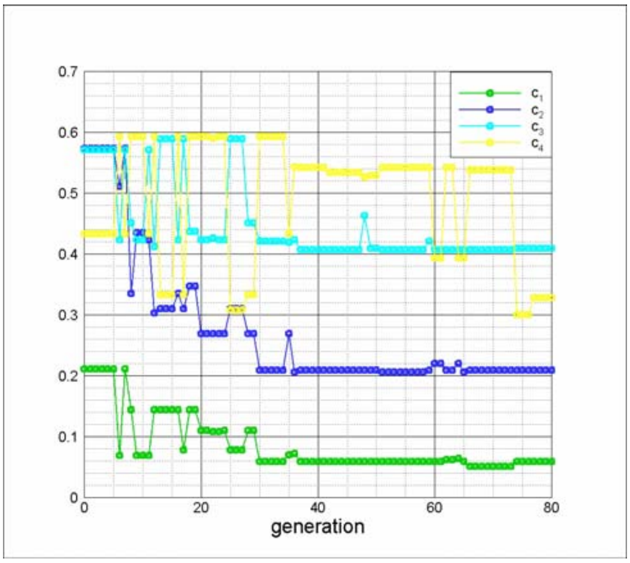

Fig. 18 c_1, c_2, c_3 and c_4 time histories

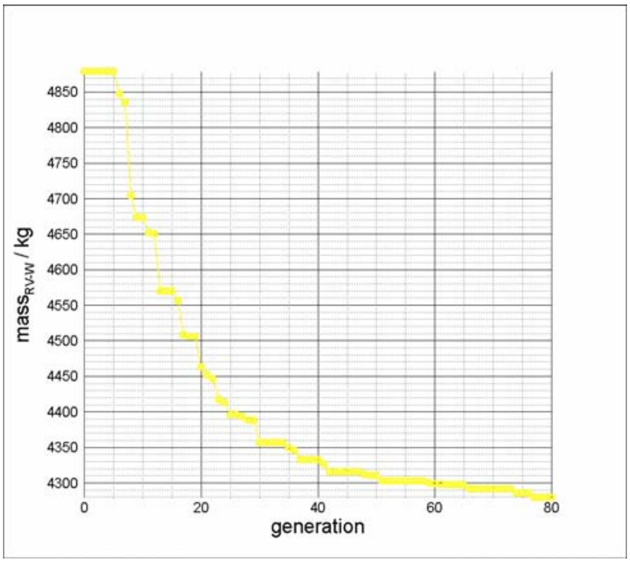

Fig. 19 RV-W mass time history

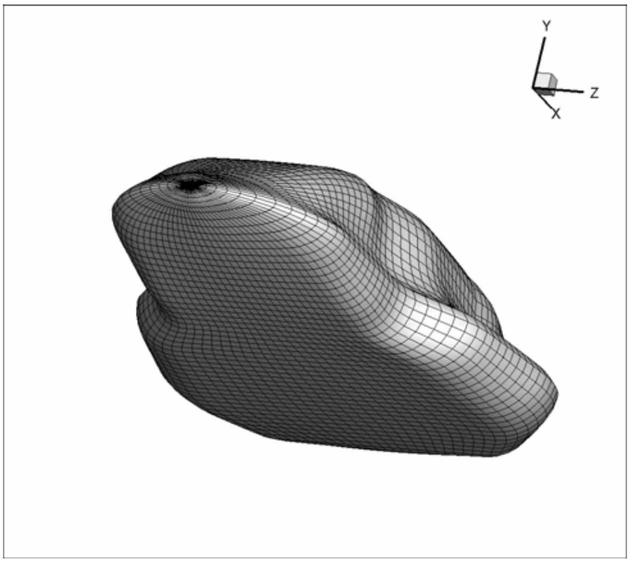

Fig. 20 Best Individual Shape at 0th Generation

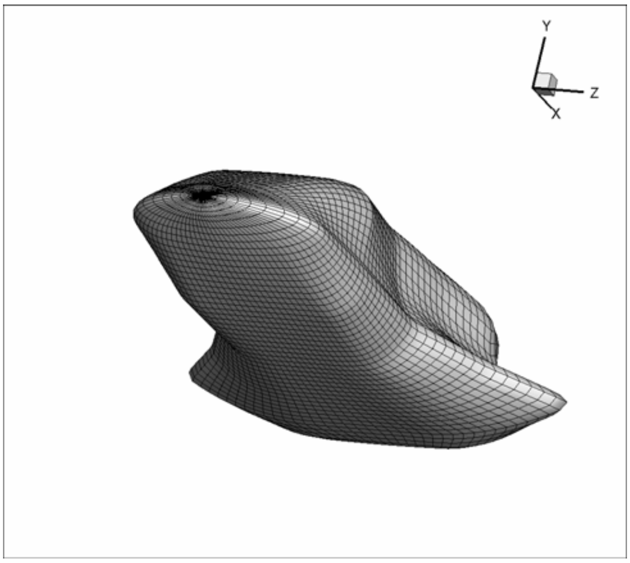

Fig. 21 Best Individual Shape at 20th Generation

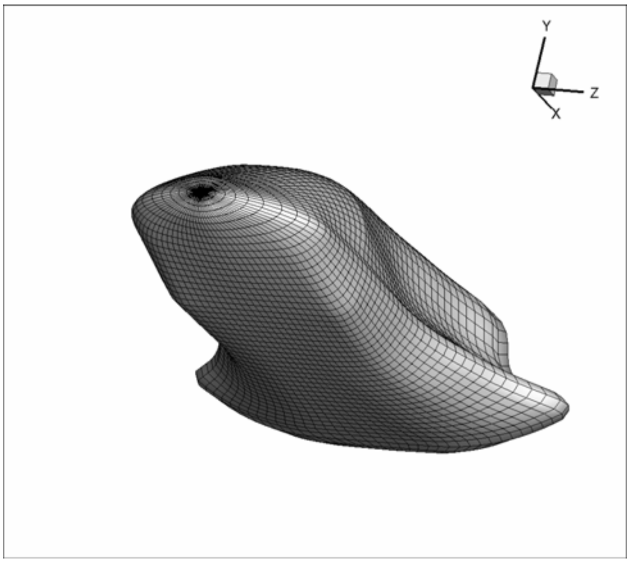

Fig. 22 Best Individual Shape at 40th Generation

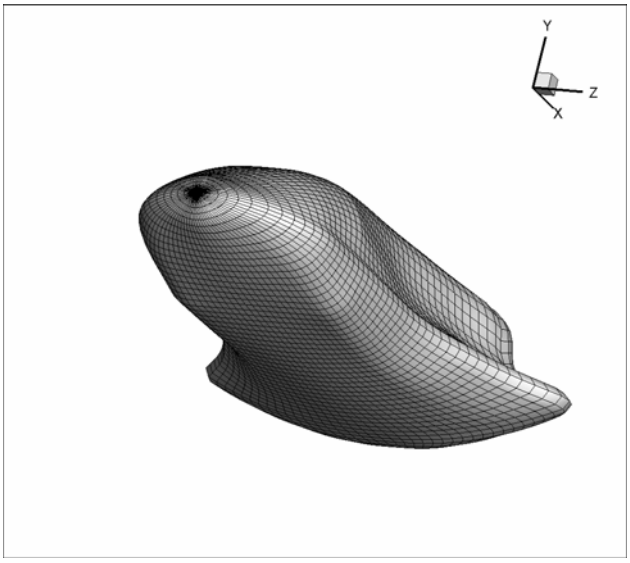

Fig. 23 Best Individual Shape at 60th Generation

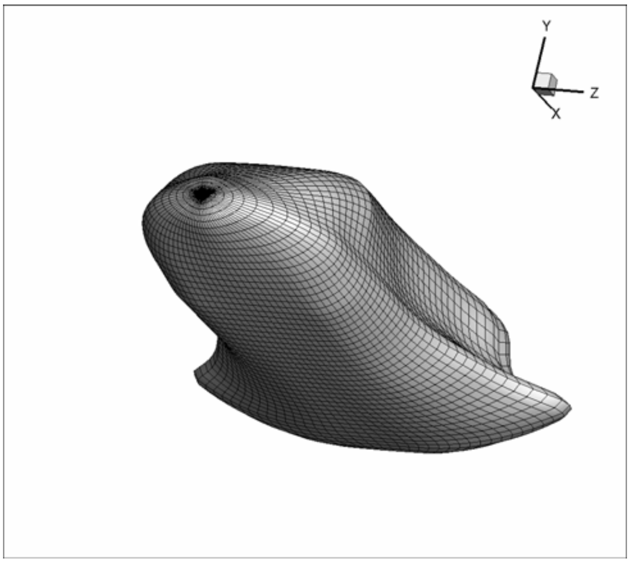

Fig. 24 Optimum Shape at the 77th Generation

The most performing RV-W configuration is found at the 77th generation: its shape is shown in Fig. 24 and its main parameters are given in Table 4.

8 Conclusions

The model and the methodologies presented suggest an approach for the RV-W shape design based on a rough but effective and computationally affordable approach to the physics of the re-entry problem. Previous paper of the authors have presented results of the mass optimization problem analyzing only the hypersonic regime of motion as the most structural and thermal demanding [11].

Table 4. Main Design Variables for the Optimum Configuration

l_1	2502.41mm
l_2	640.07mm
k_o	0.57
$k_\backslash$	1216mm
k_2	0.501
k_3	0.22
k_4	0.61
c_1	0.059
c_2	0.209
c_3	0.408
c_4	0.32
H_1	0.44
P_1	0.48
r_n	294.31mm
α	41deg

The current paper extends the analysis to the low speed flight, introducing subsonic drag parachutes, the touchdown velocity constraint and the TPS outer temperature constraint. While the RV-W mass is undoubtedly a critical parameter, the footprint is the main design performance for a RV-W. Therefore, future works will exploit capacity of the models and methods herein presented to perform a RV-W shape optimization oriented to the maximization of the footprint.

References

[1] Theisinger J.T., Braun R.D. Multidisciplinary Hypersonic Entry Aeroshell Shape Optimization. *Journal of Spacecraft and Rockets*, Vol.46, No. 5, pp 957-966, 2009.

[2] Nosratollahi M., Mortazavi M., Adami A., Hosseini M., Multidisciplinary design optimization of a reentry vehicle using genetic algorithm. *Aircraft Engin. and Aerospace Technology: An International Journal*, Vol. 82, No. 1, pp 194-203, 2010.

[3] Rohrschneider R R. "Development of a Mass Estimating Relationship Database for Launch Vehicle Conceptual Design", Georgia Institute of Technology, 2002.

[4] Cockrell D.J. *The Aerodynamics of Parachutes.* AGARD, 1987.

[5] National Aeronautics and Space Administration. *TPSX Material Properties Database*, www.tpsx.arc.nasa.gov.

[6] Hirschel E.H., *Basics of Aerothermodynamics*, Springer, 2004.

[7] Tauber M.E. *A Review of High-Speed Convective, Heat-Transfer Computation Methods*, NASA Technical Paper 2914, 1989.

[8] Schneider S.P., "Methods for Analysis of Preliminary Spacecraft Designs", Purdue University, 2005.

[9] Hirschel E.H., Weiland C. *Selected Aerothermodynamics Design Problem of Hypersonic Flight Vehicles*, Springer, 2009.

[10] Iuspa L, Scaramuzzino F. A bit-masking oriented data structure for evolutionary operators implementations in genetic algorithms. *Soft Computing,* Vol. 5, No. 1, pp. 58-68, 2001.

[11] Viviani A, Iuspa L, Lanzillo G. Preliminary Design of Minimum Configurations for a Reentry Vehicle. *3rd CEAS (Council of European Aerospace Societies) Air&Space Conference*, Venice (Italy), Paper ID 0155, pp 1984-1993, 2011.

Copyright Statement